APPLICATIONS PAPER

A CNN-Based Subpixel Level DSM Generation Approach via Single Image Super-Resolution

Yongjun Zhang, Zhi Zheng, Yimin Luo, Yanfeng Zhang, Yi Wan, Jun Wu, Zhiyong Peng and Xiu Liu

Abstract

Previous work for subpixel level Digital Surface Model (DSM) generation mainly focused on data fusion techniques, which are extremely limited by the difficulty of multisource data acquisition. Although several DSM super resolution (SR) methods have been developed to ease the problem, a new issue that plenty of DSM samples are needed to train the model is raised. Therefore, considering the original images have vital influence on its DSM's accuracy, we address the problem by directly improving images resolution. Several SR models are refined and brought into the traditional DSM generation process as an image quality improvement stage to construct an easy but effective workflow for subpixel level DSM generation. Experiments verified the validity and significance of bringing SR technology into this kind of application. Statistical analysis also confirmed that a subpixel level DSM with higher fidelity can be obtained more easily compared to directly DSM interpolation.

Introduction

With the development of earth observation technologies, we have entered an era of a remote sensing data explosion (Chi *et al.* 2016; Li *et al.* 2018; Ma *et al.* 2015), where the requirements to geographic information products are increasingly higher. Digital Surface Model (DSM), as one of the fundamental digital representations to the Earth's surface, is extremely important for both research and practical applications. And it is widely used in a variety of applications, such as building detection (Rottensteiner *et al.* 2005), city planning (Chai 2017; Yan *et al.* 2015), and environment surveillance (Sadeghi *et al.* 2016).

As high-resolution DSMs or Digital Elevation Models (DEMs) are always confidential, it is impractical to directly obtain these Geodata (Xu *et al.* 2019). So how to automatically obtain high accuracy and high resolution DSM/DEM has become a common topic in remote sensing fields (Aguilar *et al.* 2014). In recent years, instead of using high-resolution stereo/multiview image acquisition equipment, (with the existing low-resolution data to obtain high quality DSM/DEM results) seems much more economical and practical. Therefore, recent work for high-quality DSM/DEM generation mainly focused on data fusion techniques (Taud *et al.* 1999; Zhou *et al.* 2013). For example, under the framework of sparse representation, Shen *et al.* (2016) investigates DEM generation from contours. In their proposed method, a lower spatial resolution DEM and sparsely distributed contours of the same geographical area are integrated to generate a higher resolution DEM. However, in actuality, it is not easy to obtain multisource data, and it is quite complicated to register the data among various data sources, since different data sensors focus on different operating ranges and environmental conditions.

To overcome the problem of acquiring multisource data, DEM super resolution, a new concept, has been discussed in recent years. Motivated by the success of convolution neural network (CNN)-based image super resolution (SR), Xu *et al.* (2015) introduced a nonlocal algorithm to improve the resolution of an original DEM based on its partial new measurements obtained with high resolution. Later, they brought transfer learning into the task of DEM super resolution and designed a deep gradient prior network (Xu *et al.* 2019). Using this kind of method can avoid the problem of multisource data acquisition, while a new issue that model training needs abundant DEM samples is raised.

When it is impractical to obtain multisource data or enough DSM samples, how can we obtain a high quality and high-resolution DSM with low-resolution image data? The main purpose of this paper is to explore a simple but effective solution for this problem. Specifically, it takes a CNN-based SR method into traditional DSM generation process to improve image resolution, and then followed by a pixel level DSM generation process to achieve the goal of subpixel level DSM generation.

SR has been widely used in vision-related tasks. Dai *et al.* (2016) have verified the effectiveness and usefulness of SR in some vision applications, such as edge detection, semantic segmentation, digit, and scene recognition. Besides, dense image matching, a kind of method that directly operates on stereo/multi-view images, is an advisable and mainstream technology for DSM generation. And it is obvious that images data are much easier to acquire compared to the aforementioned multisource data or DEM samples. Therefore, the proposed method is much simpler and more practical compared to the aforementioned two kinds of methods in the task of generating high quality and subpixel DSM. The main contributions of this paper are as follows:

1. A simple but effective method for generating high quality subpixel DSM is proposed, which can work well without the demand of multisource data or abundant DSM samples.
2. As there is not a similar work that has been done before, some existing SR methods are refined and used in this paper to verify the feasibility of the proposed method. By comparing the experimental results, we identify the development trends of this kind of applications.

Specifically, to validate the effectiveness and usefulness of the proposed method, two aerospace image datasets from World

Yongjun Zhang, Zhi Zheng and Yi Wan are with the School of Remote Sensing and Information Engineering, Wuhan University, Wuhan, 430079, China (zhangyj@whu.edu.cn).

Yimin Luo is with the Division of Imaging Sciences and Biomedical Engineering Research, King's College London, London SE1 7EH, U.K.

Yanfeng Zhang is with the Riemann Laboratory, Huawei Technologies Co., Ltd. Wuhan 430079, China.

Jun Wu and Zhiyong Peng are with the School of Electronic Engineering and Automation, Guilin University of Electronic Technology, Guilin, 541004, China.

Xiu Liu is with the Beijing Institute of Space Mechanics&Electricity, Beijing, 100094, China.

Photogrammetric Engineering & Remote Sensing
Vol. 85, No. 10, October 2019, pp. 51–491.
0099-1112/19/51–491

doi: 10.14358/PERS.85.10.1

View and GeoEye satellites were taken to construct simulated and real data experiments, respectively. Besides, several different types of terrains were selected to test the performance of this method in different terrain conditions. Experiments verified the feasibility and practicality of this kind of application, and a subpixel level DSM with higher-fidelity can be obtained compared to directly DSM interpolation.

The rest of this paper is organized as follows: Section "Related Work" gives a brief overview on CNN-based SR methods and the applications of SR in remote sensing fields. Section "Application to Subpixel Level DSM Generation" describes the main application details and tells the evaluation metrics of the proposed approach. Section "Experiments" confirms the effectiveness and practicability of this kind of application with simulated experiments and real data experiments. Finally, the "Conclusion" section concludes this paper.

Related Work

In this section, we will introduce and analyze related methods on image super resolution and give a brief overview on some relevant applications of SR technology in remote sensing fields.

Image SR

Image SR aims to restore a high-resolution (HR) image from one or more low-resolution (LR) images. Numerous methods have been proposed to deal with the image SR problems in recent years, which can be mainly classified into reconstruction-based SR and learning-based SR (Zeng *et al.* 2017).

The reconstruction-based SR methods assume that the LR images are from the observations of their related LR images after transformation, deformation, and noise disturbance. As SR is an ill-posed task, reconstruction-based methods attempt to optimize the problem by imposing some extra assumptions, such as smoothness and limited bands *(*Sun *et al.* 2008*;* Tai *et al.* 2010; Zhang *et al.* 2010). However, the added assumptions will heavily limit the performance of this kind of method since they are always unsuitable in most image situations.

Different from the reconstruction-based methods, the learning-based SR methods learn the high frequency information difference through constantly training high/low-resolution image pairs, and then build a robust model. After that, given a low-resolution image into the learned model, its corresponding HR image can be restored. Specifically, according to the different strategy of learning, the learning-based method can be further divided into sparse-coding-based methods(Yang *et al.* 2008;Yang *et al.* 2010), manifold-learning-based methods(Chang *et al.* 2004; Lu *et al.* 2013) and CNN-based methods(Dong *et al.* 2016; Kim *et al.* 2016). Since more high-frequency details can be learnt from the numerous image samples, CNN-based methods visibly outperform other methods. A pioneer work of CNN-based SR methods is called super-resolution convolution neural network (SRCNN) (Dong *et al.* 2016), which learns an end-to-end nonlinear mapping between LR and HR image pairs via a three-hidden-layers CNN architecture. However, this method cannot extract satisfactory image feature for HR image reconstruction due to the shallow architecture. Considering this, Kim *et al.* (2016) developed a much deeper SR model Very Deep Super Resolution (VDSR), of which the number of convolution layers is increased to 20. As the difference of LR/HR image pairs are mainly located in high frequency part, Kim *et al.* (2015) proposed another network Deeply-Recursive Convolutional Network, which utilized residual learning (He *et al.* 2016) as optimization strategy to accelerate the convergence speed of their proposed network. Bicubic down-sampling is commonly used in these CNN-based methods to generate LR images from their HR counterparts, which results in the unsatisfactory performance on real data. Therefore, Zhang *et al.* (2018) proposed an effective model super-resolution network for multiple degradations (SRMD) to address this problem to some extent, which established a degradation formula between the HR/LR image pairs and took the LR images and the degradation maps as input to reconstruct the corresponding HR results.

SR in Remote Sensing Fields

As an effective technology for improving image spatial resolution, image super resolution is highly related to remote sensing fields. And some classical SR methods in computer vision fields were transferred into remote sensing fields to better solve those ill-posed problems. Luo *et al.* (2017) refined Very Deep Super Resolution (VDSR) to deal with image compression problem that occurred during video satellite image transmission process, Song et al (2018) applied SRCNN to image fusion tasks as a transitional image generation tool, and He *et al.* (2018) adopted cascaded deep network and multiple receptive fields for infrared image super resolution. Besides, considering the special characteristic of remote sensing images, Huang et al (2017) developed remote sensing deep residual-learning specifically for remote sensing images super-resolution, while Lei *et al.* (2017) used local-global combined network (LGCNet) to learn multilevel representations of remote sensing images. Moreover, Jeon *et al.* (2018) utilized a parallax prior in stereo images to reconstruct HR images for subpixel registration accuracy, and Song *et al.* (2016) extended the success of deep convolutional neural network to depth image super resolution.

To the best of our knowledge, even though SR methods are widely applicated into remote sensing fields and Dai *et al.* (2016) have already verified the effectiveness and usefulness of SR technology in several vision applications, there is not a work to discuss whether it is feasible to bring the SR method into traditional dense matching procedures for obtaining subpixel level DSM.

Since the main purpose of this paper is to explore the feasibility and practicality of this kind of application and to show the effect of bringing different SR models into the framework, for fair comparison and better explaining the experimental results, we refined several SR models to show the performance difference and analyze the practicality of the proposed method in this paper, rather than designed a new SR model.

Application to Subpixel Level DSM Generation

As illustrated in Figure 1, the workflow of this application can be mainly divided into two stages. Separately, in step I, the image quality and spatial resolution is improved by CNN-based SR module. The SR module is adopted to enhance the object texture and edge detection, which helps extract more reliable matching points for subsequent DSM generation process. Then, with the obtained HR images from step I as input, a subpixel level DSM with high fidelity can be obtained from a standard DSM generation procedure in step II. In this section, the details of this application will be explained in the following aspects: refinement details of SR models, DSM generation process, and quality assessment metrics.

Refinement of SR Models

In this subsection, we will introduce how to reconstruct a HR image from its counterpart LR image. For the ease of representation, the LR image is denoted as x_i, its corresponding HR image is denoted as y_i, and y_i' is the reconstructed result of LR image through CNN architecture. Specifically, x_i is obtained from y_i according to down-sampling or a special degradation formula. Therefore, as illustrated in Figure 2, a robust architecture can be obtained by repeatedly minimizing the difference between HR image y_i and y_i'. To measure the difference between real HR image y_i and predicted HR image y_i', mean squared error (MSE), is usually used as Equation 1,

$$\mathrm{MSE} = \frac{1}{\mathrm{width} \times \mathrm{height}} \left\| y_i - y_i' \right\|^2 \tag{1}$$

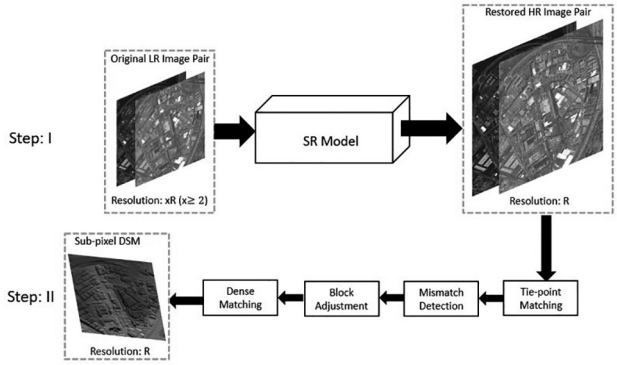

Figure 1. Flowchart of the application to subpixel level DSM generation.

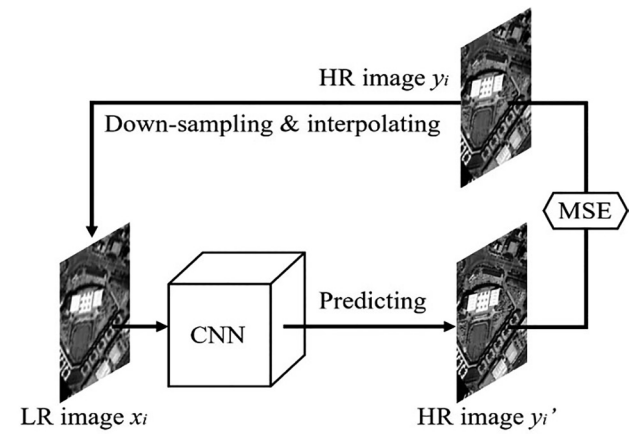

Figure 2. CNN architecture for SR.

In this paper, four different methods are adopted and refined to improve the image quality and spatial resolution, one of them is bicubic-upscale interpolation, and the other three are CNN-based SR methods SRCNN, VDSR, and SRMD. To train a robust CNN architecture specially for remote sensing images, both natural images and aerospace images are selected as network training samples to retrain the refined model for improving network adaptability.

Due to the special calculating operation of convolution, it will cause serious information loss at image border, while it is necessary to keep the same size between the input and output images in this application. As used in many papers, border padding before convolution operation is an effective way to deal with the problem. Kim *et al.* (2016) padded zeros around the original image before each convolution layer to make the output have the same size as the input. However, the zero-padding method inevitably bring some useless information or even jeopardize the reconstruction of images. In our previous work (Luo *et al.* 2017), we calculated the size difference between the input and output according to convolutional kernel and stride of each convolutional layer, and proposed to use symmetric padding as a substitute to alleviate the information loss at image border. In this paper, to further avoid information loss and useless information taken-in for a better DSM, we refined the SR models by applying symmetric padding before each convolution layer for better capturing image information rather than just used it at the very beginning.

DSM Generation

All the mentioned approaches regarding to DSM generation are the previous achievements of our research team, which makes a good foundation for the verification of the proposed subpixel level DSM generation application. We will give a brief overview on how to construct the DSM generation procedure in this subsection.

As illustrated in Figure 1, this DSM generation procedure contains four main steps: tie-point matching, mismatch detection, block adjustment, and dense image matching.

Firstly, tie-point matching is used to find corresponding points in a pair of images (even in multiple images). Considering that images used for DSM generation may come from different remote sensing sensors, a tie-point matching algorithm for multisource images (Ling *et al.* 2016) is implemented for corresponding points identification. After that, to produce reliable matching results, a region segmentation based matching propagation strategy is designed in this algorithm, so that more corresponding points for afterwards process can be obtained.

Secondly, considering the mismatch situation caused by tie-point matching process, a mismatch detection method should be brought into our DSM generation procedure. Wan *et al.* (2017) proposed an effective mismatch detection method for push broom high-resolution satellite images, named point-to-line distance based (P2L) method. This method can distinguish most of the mismatches, even for the image pairs which have a 54-degree intersection angle. Therefore, we take it for our mismatch detection process.

At last, with the selected corresponding points, we constrain the elevation of each tie point for the sake of relative geometric rigidity based on a DEM-Assisted rational function model (RFM) (Zhang *et al.* 2016). And a robust dense image matching method named semiglobal vertical line locus matching (SGVLL) is taken for the DSM generation (Zhang *et al.* 2017).

Besides the aforementioned procedure, there is another important step to this application, which is called rational polynomial coefficient (RPC) regeneration. (RPC files describes the correlation between satellite images and three-dimension objects and are necessary for image matching. As different satellite images have different RPC files, the RPC files also need to be regenerated when the images are super-resolved. The procedure of regenerating RPC files is as follows:

1. With the original RPC file and LR image, the relationship between the LR image and a virtual three-dimensional grid can be established, so the geographic position of the grid can be described.
2. With the virtual three-dimensional grid and new sample parameters, the new RPC file can be regenerated.

Quality Assessment Metrics

Image quality refers to visually significant attributes of images. As images with higher quality can offer better image texture for subsequent process, it is necessary to evaluate the images quality before taking them into the DSM generation process. To evaluate the performance of the quality of reconstructed methods, peak signal-to-noise ratio (PSNR) and structural similarity index (SSIM) are selected as quantitative metrics. PSNR (in dB) and SSIM are calculated in Equations 2 and 3:

$$\mathrm{PSNR} = 10 log_{10} \frac{\left(2^n - 1\right)}{MSE} \tag{2}$$

where MSE is defined in Equation 1.

The calculation of SSIM is based on three relatively independent indicators, namely luminance, contrast, and structure. SSIM is defined as follows:

$$\mathrm{SSIM}\left(I,I\right) = \left[C_l\left(I,I\right)\right]^{\alpha}\left[C_c\left(I,I\right)\right]^{\beta}\left[C_s\left(I,I\right)\right]^{\gamma} \tag{3}$$

where I and $\hat{I}$ are two images to be compared. α, β, γ are control parameters for adjusting the relative importance and $C_l(I,\hat{I})$, $C_c(I,\hat{I})$, $C_s(I,\hat{I})$ are comparison functions on luminance, contrast and structure, respectively. Specific introduction of $C_l(I,\hat{I})$, $C_c(I,\hat{I})$, $C_s(I,\hat{I})$ can be found in Wang *et al.* (2019).

The range of SSIM is [0:1]. With higher SSIM, the reconstructed images are more similar to the real HR images. Although there is not a specific range of PSNR, it follows the same trend with SSIM, which means the higher PSNR indicates better image quality.

For the evaluation of DSM quality, two indicators are used in this paper, namely root-mean-square error (RMSE) and mean relative error (MRE). Suppose the reference DSM as D and the DSM from reconstructed images as C, so that D and C are two components that need to be compared. RMSE and MRE for DSM quality assessment can be expressed as Equations 4 and 5, respectively.

$$\mathrm{RMSE}(C,D)=\sqrt{\frac{1}{N}\sum_{i=1,j=1}^{i=n,j=n}\left(C_{ij}-D_{ij}\right)^2}, \tag{4}$$

$$\mathrm{MRE}(C,D)=\frac{1}{N}\sum_{i=1,j=1}^{i=n,j=n}\frac{\left|C_{ij}-D_{ij}\right|}{D_{ij}}, \tag{5}$$

where N stands for the number of a DSM matrix's element, and (i, j) represents the position at i^{th} row and j^{th} column. To measure the performance difference of the different SR models, RMSE and MRE between reconstructed DSMs and the reference DSM are calculated. The lower RMSE and MRE indicate that the reconstructed DSM is more similar to the reference DSM, which are regarded as a better DSM.

Experiments

This section constructs simulated and real data experiments to verify the feasibility and practicability of the proposed method for subpixel DSM generation. It can be divided into three subsections, namely experiment details of image SR, simulated experiments, and real data experiments.

Experiment Details of Image SR

This subsection aims to describe the details of stage I of the proposed method and compared the results of reconstructed HR images.

Training Details

To train these SR models, an augmented training dataset was used. The training dataset contained 291 natural images in (Schulter *et al.* 2015) and 109 very high-resolution aerial images from the Dataset for Object deTection in Aerial images (DOTA) dataset (Xia *et al.* 2018). The mixed dataset was randomly split into 1 325 000 standard image patches for training. Moreover, to ensure the size of the output images unchanged, symmetric padding was added before each convolution layer to refine these CNN-based SR methods. The training process was implemented on Caffe Library (Wen *et al.* 2016).

Image Reconstruction

With the trained models, the LR aerospace images were taken as input to obtain reconstructed HR images. Specifically, as remote sensing images were always in huge size, it was necessary to divide them into patches for practical use. After that, the reconstructed HR images would be merged back according to their original order. Besides, the image reconstruction process was based on MatConvNet (Vedaldi and Lenc 2015).

Results Comparison of Super-Resolved Images

To show the texture difference of the reconstructed images, a building was selected and enlarged to show the visual difference of the super-resolved images in Figure 3. Besides, several regions from our tested image dataset were selected to present the performance difference of these SR models, and the quantitative PSNR and SSIM results were shown in Table 1. From the visual difference of the red ovals in Figure 3, it could be found that some small objects/texture could be reconstructed correctly with VDSR and SRMD, while bicubic and SRCNN could not obtain the same result. And the statistical evaluation further showed that SRMD outperformed the other methods, while bicubic performed worst. It was worth noting that the image texture was of significance in the subsequent image matching process, so it could be forecasted that with a better SR model, the quality of the corresponding DSM would be better.

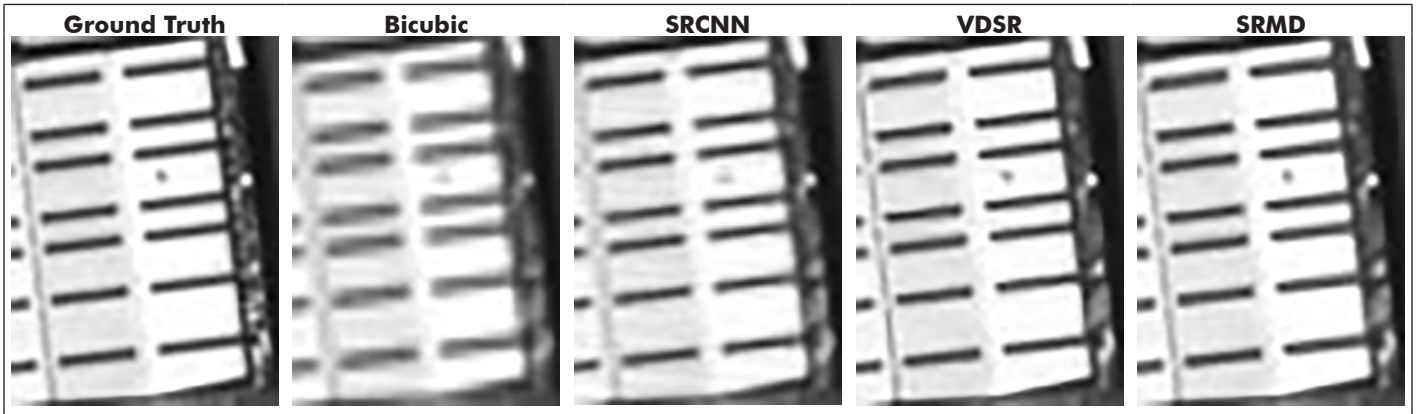

Figure 3. Visual comparison of the reconstruction results among different SR models (the red ovals: reconstruction results of a small object on the building roof).

Table 1. Stereo images quality assessment (left/right).

Method	Bicubic		SRCNN		VDSR		SRMD	
Regions	PSNR	SSIM	PSNR	SSIM	PSNR	SSIM	PSNR	SSIM
A	29.98/32.28	0.8172/0.8453	32.15/35.21	0.8832/0.9135	33.50/36.99	0.9235/0.9609	**34.79/37.66**	**0.9696/0.9754**
B	34.35/34.95	0.7728/0.8679	36.03/37.49	0.7977/0.9246	38.50/37.87	0.9040/0.9617	**39.00/38.92**	**0.9759/0.9699**
C	38.75/38.14	0.7405/0.8278	39.73/40.15	0.7382/0.9130	41.42/41.00	0.9146/0.9639	**42.40/42.47**	**0.9772/0.9699**
D	40.10/37.09	0.5932/0.8770	40.41/39.20	0.6740/0.9147	43.10/39.80	0.8828/0.9582	**44.25/40.05**	**0.9864/0.9628**

Simulated Experiments

Experiments Data

To better validate the feasibility and practicality of this kind of application, a series of simulated experiments were conducted on World View stereo image dataset at first. The dataset was established with left images from WorldView1 and right images from WorldView2, of which the spatial resolution was 0.5 m. Besides, the geographical positioning accuracy of the dataset was 4.1 m with circular error at 90% probability. The testing site of this paper was located at Terrassa, Spain which covered a semirural area at undulating terrain.

Experiments Details and Results

In this subsection, the LR images were downscaled from the HR images with bicubic down-sample. As more information would be lost with a larger downscale factor and the main purpose of the paper was for experimental validation, we just set the downscale factor as 2 to conduct all the experiments. Besides, as the super-resolved images had the same spatial resolution and size with the original HR images, it was unnecessary to regenerate the RPC files in this subsection.

Under these conditions, the main experimental procedure for subpixel DSM generation in this subsection was as follows: the original HR stereo images were used to generate a reference DSM at first. Then, the downscaled images were super-resolved with different SR models. The DSMs with super-resolved images from different SR models were then generated. Moreover, to further demonstrate the superiority of generating high-fidelity subpixel level DSM, directly DSM upscale results were added as extra comparison experiments, where the LR DSMs were firstly generated with the downscaled image pairs and then interpolated to the same resolution with the reconstructed DSMs.

Based on the consideration of time-consumption and DSM accuracy, a coarse-to-fine pyramidal DSM procedure was adopted for generating a high accuracy DSM. In this process, with/without the assistance of shuttle radar topography mission (SRTM), the oriented super-resolved stereo images were used to generate a relative low-resolution DSM at first, so that the elevation range of the main terrain in the site could be roughly determined. Then, with the guidance of the coarse DSM, a relatively fine DSM could be obtained via repeating the dense matching process. By iterating the coarse-to-fine step, a DSM which had the same resolution as the HR images could finally be obtained. In addition, a DSM refinement strategy was taken after each coarse-to-fine step to further optimize the generated DSM.

It was worth noting that the spatial resolution of the finally obtained DSMs were the same as the super-resolved images, which was subpixel level compared to the LR images, therefore we regarded it as subpixel level DSM in this paper.

To show the performance of the application, four regions of different terrains were selected to produce DSMs, whose spatial resolution were 0.5 m. The generated DSMs were shown in Figure 4, where the first DSM represented the reference DSM in each region, the second represented the DSMs from LR DSM upscale, and the others represented the DSMs generated with different reconstructed HR images. Quantitative evaluation results for calculating deviation of these DSMs to their reference DSM were counted in Table 2.

Experiments Analysis

For the ease of illustration, DSMs generated from reference HR images were denoted as "Ref-DSM". DSMs generated from different super-resolved images were denoted as "Bi-DSM",

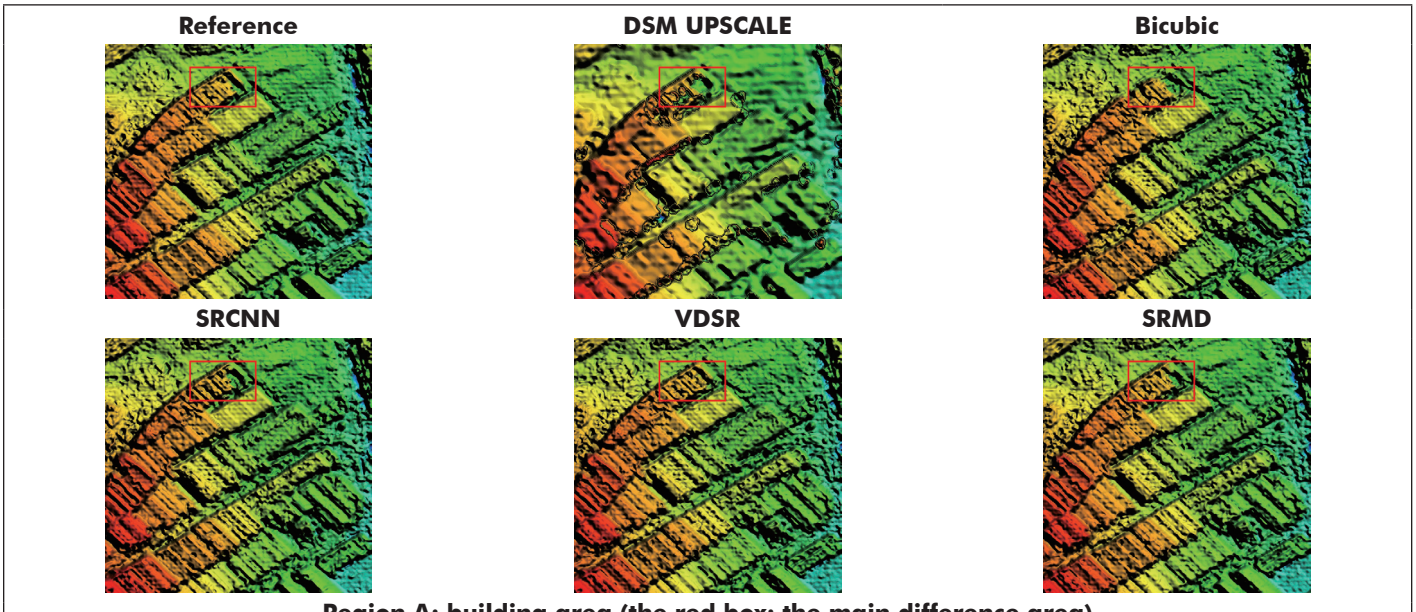

Figure 4. Comparison of generated DSMs from different methods in four regions of several different types of terrain. (Region A is a building region, region B is a mountain region, region C is a main road region, and region D is a special region which contained mismatch). *Continued on next two pages.*

Table 2. Quantitative evaluation of reconstructed DSMs.

Regions (region size)	Methods									
	DSM UPSCALE		BICUBIC		SRCNN		VDSR		SRMD	
	RMSE (m)	MRE/%	RMSE (m)	MRE/%	RMSE (m)	MRE/%	RMSE (m)	MRE/%	RMSE (m)	MRE/%
A (604 * 634)	29.2777	2.64	1.2374	0.16	0.9455	0.14	0.7425	0.11	**0.7249**	**0.08**
B (892 * 806)	82.1113	6.36	87.9862	8.77	53.9941	3.79	46.4107	3.02	**35.7335**	**1.91**
C (895 * 671)	131.1828	13.46	118.8005	17.83	103.1256	11.43	84.3968	9.9	**76.0433**	**6.45**
D (1544 * 859)	53.4419	7.18	12.1617	1.35	12.1557	1.34	9.43	1.03	**7.1771**	**0.71**

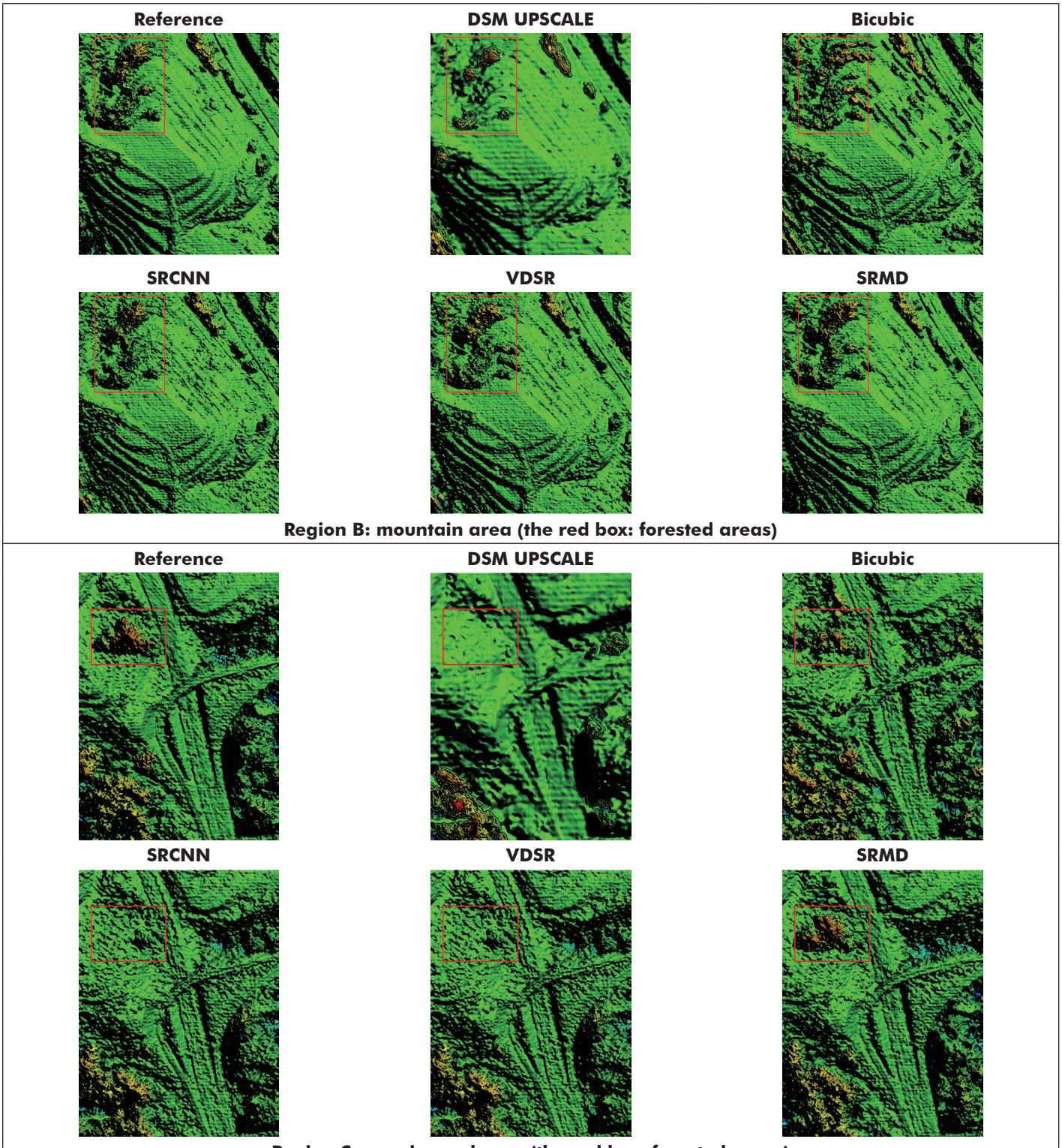

Figure 4 *continued*. Comparison of generated DSMs from different methods in four regions of several different types of terrain. (Region A is a building region, region B is a mountain region, region C is a main road region, and region D is a special region which contained mismatch). *Concluded on next page.*

"SRCNN-DSM", "VDSR-DSM", and "SRMD-DSM". And all the DSMs obtained from CNN-based SR models were denoted as "SR-DSMs".

Generally, it was obvious that the CNN-based methods could generate better subpixel level DSMs in any terrain situations compared to directly DSM upscale from Table 2. And the results in Figure 4 also showed that the DSMs obtained from the proposed method had higher fidelity and contained more terrain details. Besides, as the SR-DSMs were obtained from higher-resolution image pairs, there were less mismatch compared to the directly DSM upscale results.

For the sake of comprehensiveness, both subjective and objective evaluations were taken into consideration for analysis. Subjectively, in Figure 4, the selected four regions could be mainly divided into three parts: building areas (region A), nonbuilding

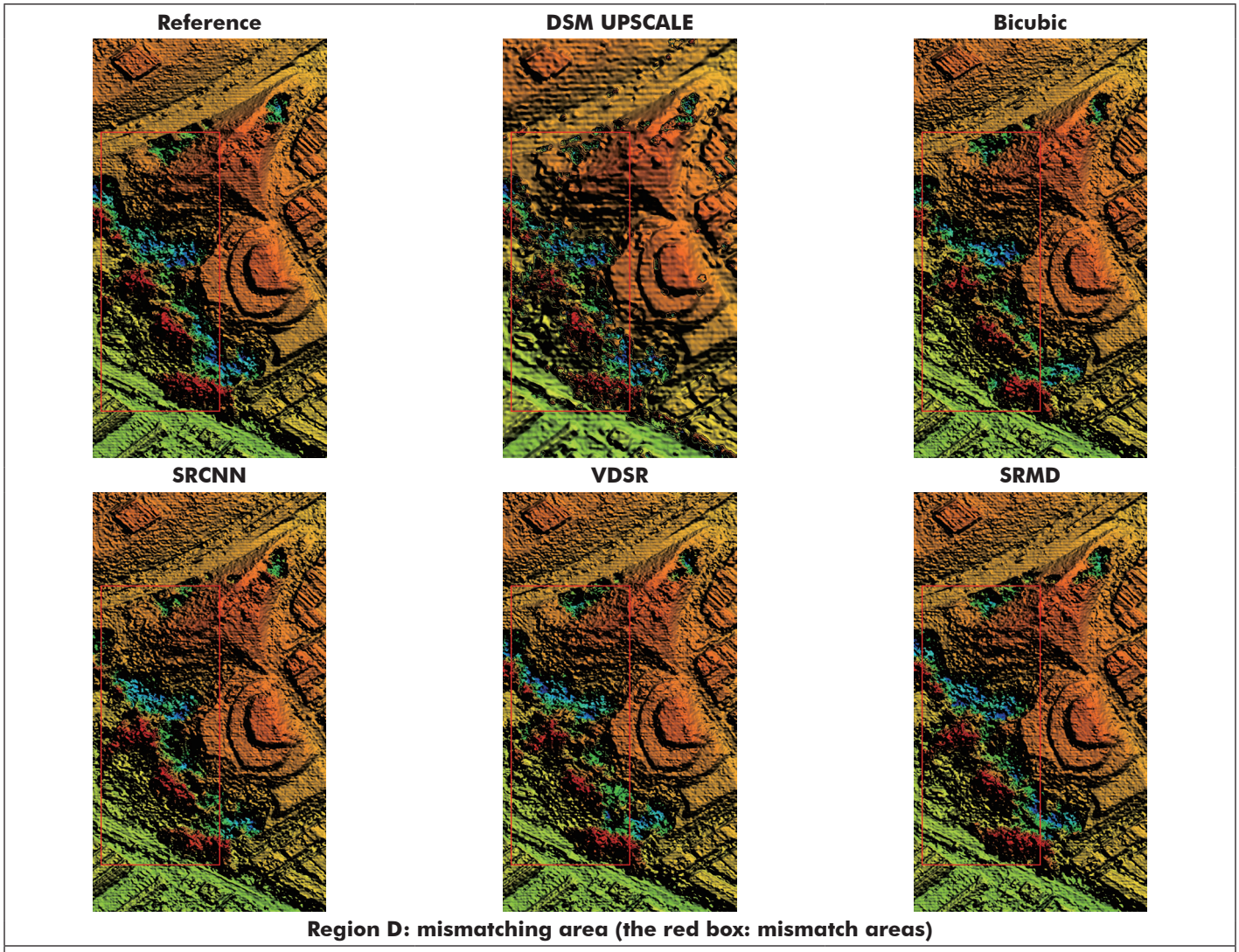

Figure 4. Comparison of generated DSMs from different methods in four regions of several different types of terrain. (Region A is a building region, region B is a mountain region, region C is a main road region, and region D is a special region which contained mismatch).

areas (region B, C), and a special mismatching area (region D) which contained both building area and nonbuilding area.

Firstly, it seemed that the SRMD-DSMs were always the closest results to the corresponding Ref-DSMs, even in the mismatched region, which indicated that SRMD could achieve the best performance among these image reconstruction models no matter which type the terrain belongs to. The conclusion was the same to the image reconstructed results shown in Table 1 and Figure 3. This indicated that the generated DSM would be better with a better SR model, so the problem of DSM quality improvement might be converted into an easier image SR problem.

Secondly, in the building region (region A), the quality difference among these DSMs were slight and nearly invisible. It was explainable as the resolution of used images were high enough (0.5 m), so enough accurate feature points in the building edge could be obtained for subsequent DSM generation. Even when most of this region seemed to be the same, DSM upscale and bicubic methods failed to reconstruct the complete building in the red box, while all CNN-based SR methods could obtain the whole building edge, and the result of SRMD was nearly same to the reference. On the contrary, the visual difference was more distinct in nonbuilding regions (region B, C) among the SR-DSMs. For example, in the red box of region B and C (both belong to vegetation covered areas), BI-DSMs performed the worst and even could not reconstruct the correct terrain, while all the SR-DSMs could, more or less. And compared to the DSM upscale method, CNN-based SR models were more robust and less likely to produce incorrect results. It was because more terrain features and mapping relationships were learned from the samples when training these models, thus the reconstructed images could represent the real terrain better. All the results confirmed the significance of enhancing image texture for better DSMs generation, and further verified the feasibility of the proposed application.

Objectively, as illustrated in Table 2, in nonbuilding regions, CNN-based SR models always outperformed the bicubic upscale method, especially in some complex terrains, e.g. the red box area of region C. As shown in Table 2, the RMSE and MRE of this region were even up to 118.8005 and 17.83% in BI-DSM, while the SR-DSMs had lower RMSE and MRE. In particular, the SRMD-DSM reached the lowest RMSE and MRE, which was just about 2/3 and 1/3 of the BI-DSM. However, even though the experimental results clearly verified that the SRMD method could obtain a much better DSM than the direct upscale method, it must be noticed that the RMSE results of region B and region C were still too high. As the abnormal RMSE occurred with vegetation covered regions (region B, C), we constructed further experiments to investigate the specific reason. Partial experiment results are shown in Figure 5 and Table 3.

Considering that dense matching algorithms always failed at forested terrains, which might result in unknown elevation deviation and abnormal RMSE, we removed most of vegetation covered areas from region B in Figure 4 to see whether the abnormal RMSE situation could be partially solved. The new experiment region is shown in Figure 5, and the quantitative results are in Table 3. As displayed in Table 3, the RMSE results had improved a lot after removing vegetation covered area, which explained the abnormal RMSE situation in Figure 4.

Moreover, VDSR and SRMD were regarded as two different optimizing strategies of the basic CNN-based SR model (SRCNN) in this paper, of which the former tried to add layers and adjusted network architecture while the later focused on exploring image degradation formula. The experimental results shown in Table 2 confirmed that when the SR model was optimized, the DSMs quality could be improved. That is to say, compared to directly DSM upscale, a more satisfactory subpixel level DSM could be obtained with a CNN-based SR model. Furthermore, by optimizing the SR methods, the DSM

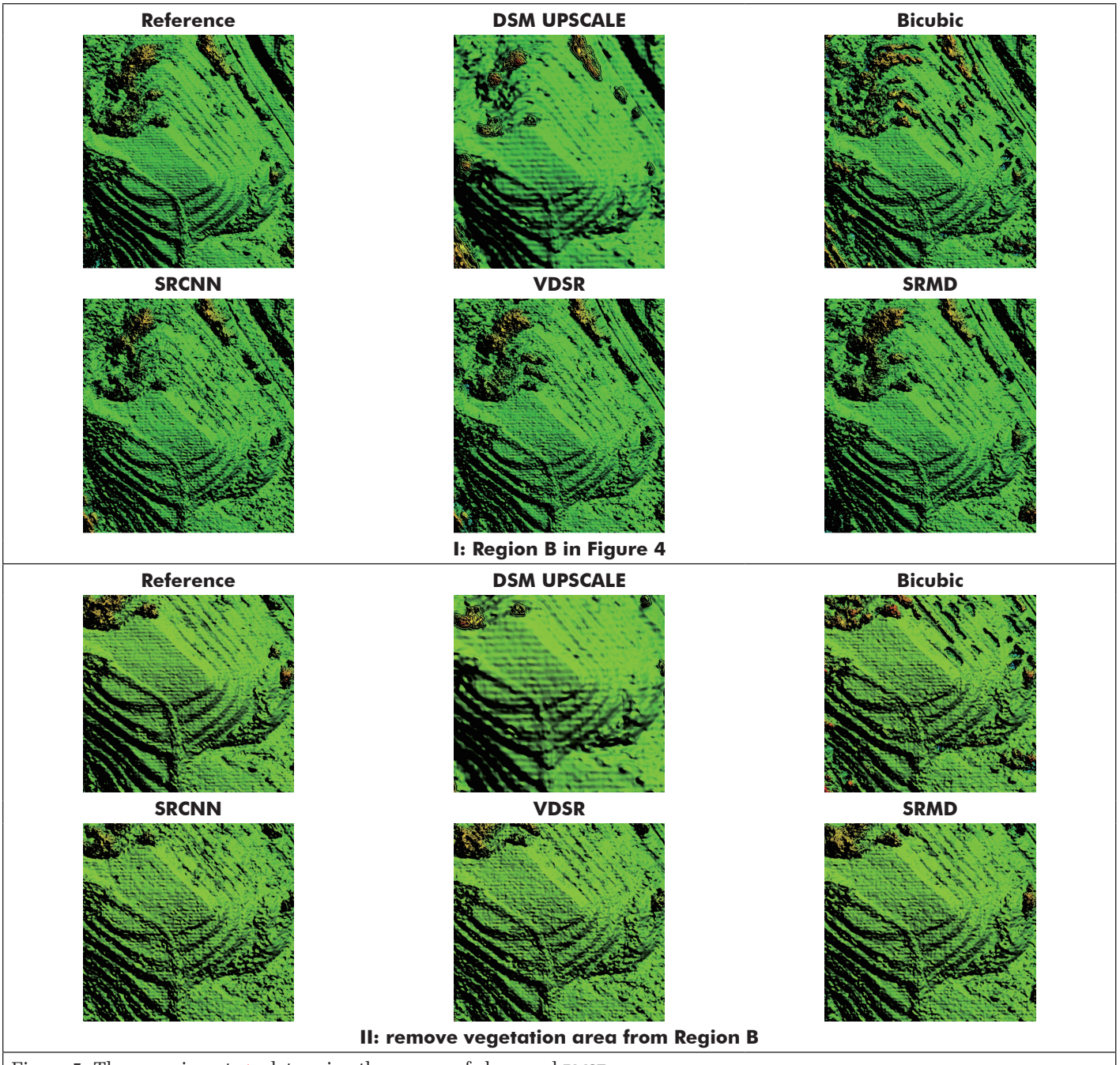

Figure 5. The experiments to determine the reason of abnormal RMSE.

Table 3. Quantitative evaluation of experiments in Figure 5.

Methods	DSM UPSCALE		BICUBIC		SRCNN		VDSR		SRMD	
Regions (region size)	RMSE(m)	MRE/%	RMSE(m)	MRE/%	RMSE(m)	MRE/%	RMSE(m)	MRE/%	RMSE(m)	MRE/%
I: (892 * 806)	82.1113	6.36	87.9862	8.77	53.9941	3.79	46.4107	3.02	**35.7335**	**1.91**
II: (668 * 626)	29.8961	1.18	48.7352	3.55	24.1997	0.96	18.5257	0.7	**16.8759**	**0.69**

results could also be optimized, which indicated the quality of generated DSM could be converted to the task of image quality promotion.

Real Data Experiments

The previous subsection validated the feasibility and practicality of the proposed method for subpixel generation. This subsection focused on its effectiveness and usefulness on real image data.

Experiments Data

In this subsection, the image data from GeoEye satellite with real image degradation relation were used to evaluate the proposed method. Different from the simulated experiments, the LR stereo images used here were real images taken at the same time with their counterpart HR images, rather than generated from the original HR images. The images were taken in California, United States, with 0.5 m resolution for HR images and

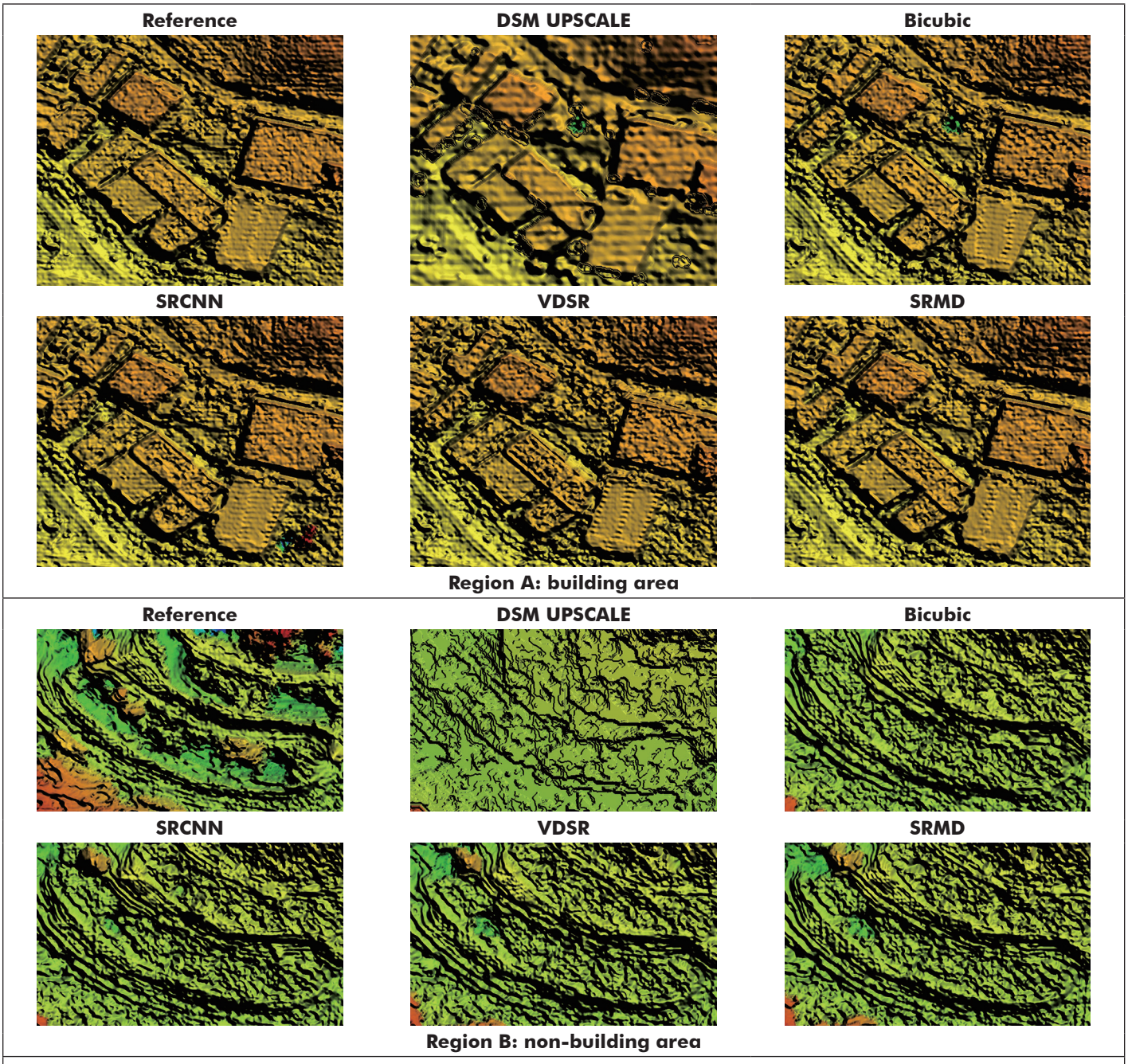

Figure 6. Visual comparison of reference DSMs and DSMs from different methods (region A is a building region; region B is a forested and easy-mismatched region).

Table 4. Quantitative evaluation of reconstructed DSMs.

	Methods									
	DSM UPSCALE		BICUBIC		SRCNN		VDSR		SRMD	
Regions	RMSE(m)	MRE/%	RMSE(m)	MRE/%	RMSE(m)	MRE/%	RMSE(m)	MRE/%	RMSE(m)	MRE/%
A (550 * 674)	24.7955	1.74	2.7447	0.22	3.6123	0.23	1.2113	0.17	1.1252	0.13
B (396 * 666)	59.3723	4.43	58.5283	4.25	57.7189	4.08	55.5158	3.87	54.7113	3.79

2 m for LR images. The LR images were multispectral images, while the HR images were panchromatic images.

Experiment Details and Results

In this subsection, the LR multispectral image pairs were firstly composited to single-channel images. After that, the obtained image pairs were super-resolved with different image reconstruction models. The original HR images were taken to generate reference DSM, and the reconstructed HR images were taken to generate reconstructed DSMs, with 0.5 m resolution. It is worthwhile to note that the RPC files of the reconstructed images needed to be regenerated from the RPC files of the original LR images.

In this subsection, we selected two different regions to display the experiment results. One was building region, which was used to demonstrate the robustness of the proposed framework in the building region; the other one was a complex terrain which contained forested and easy-mismatched areas. The visual comparison results are shown in Figure 6, and the quantitative evaluation results are shown in Table 4. Also, an extra experiment, which generated LR DSMs from composited LR image pairs and upscaled four times to the resolution of the reference DSMs, was set as comparison experiment for real image situations.

Experiment Analysis

The visual comparison in Figure 6 and quantitative results in Table 4 also had the same experimental conclusion as the simulated experiments. Moreover, as shown in region B of Figure 6, even though the statistical results of RMSE and MRE were abnormal at the complex terrain, the visual comparison and quantitative results still confirmed that the proposed framework could generate better subpixel level DSMs. Therefore, the proposed framework was certainly effective and useful in real image conditions.

Besides, it should be illustrated that the DSMs in real image data among these models were less satisfactory than the simulated experiments. For example, the RMSE deviation between VDSR-DSM and SRMD-DSM in region A and B were only about 0.09 m and 0.8 m. The main reasons are two-fold:

Firstly, the SR models adopted were actually designed for bicubic downscaled LR images, while the degradation relationship between the HR images and composited LR images were not such simple.

Secondly, the composited images also had some information difference with the panchromatic images, which were jeopardized for obtaining well-performed results. Therefore, though SRMD had taken some imitated noise and degradations into consideration, the final results were still less significant than the simulated experimental results.

Conclusion

In previous research work, subpixel level DSM generation mainly relied on multisource data fusion or DSM super-resolution, which raised the problem of acquiring different sources and different types of data, or the demand of abundant DSM samples. To shake off the reliance on multisource data or plenty of DSM samples, this paper proposed a simple but effective framework to generate subpixel level DSM with high quality and high fidelity. Specifically, as DSMs from dense matching methods depend a lot on the original aerospace images, we take the CNN-based method into the traditional DSM generation process as an image quality improvement strategy, then generate a high-fidelity and subpixel level DSM. The experiments verified the feasibility and practicality of the proposed framework and presented the high-fidelity and subpixel level DSM results. Besides, statistic results also confirmed the visibly superiority of the proposed method to directly DSM upscale method under most terrain conditions.

However, the method proposed in this paper is just a first trial of generating subpixel level DSM in the framework of improving the original image quality through SR models. The result is preliminary, so more experiments are needed to dem-onstrate its practicability. Besides, there is still much room for improvement. For example, a new SR model which exploits the actual degradations between the corresponding HR and LR images needs to be developed to improve the performance. Moreover, the reference in all of our experiments is better to be replaced by ground truth to avoid unknown errors during the Ref-DSM generation procedure. These issues will be ad-dressed in our future work.

Acknowledgments

This work was supported by National Natural Science Foundation of China with project number 41871368 and 41571434 and National High-score Major Special Projects of China with project number 50-H31D01-0508-13/15.

References

Aguilar, M. A., M. del Mar Saldana and F. J. Aguilar. 2014.Generation and quality assessment of stereo-extracted DSM from GeoEye-1 and WorldView-2 imagery. *IEEE Transactions on Geoscience and Remote Sensing* 52:1259–1271.

Chai, D. 2017. A probabilistic framework for building extraction from airborne color image and DSM. *IEEE Journal of Selected Topics in Applied Earth Observations and Remote Sensing* 10:948–959.

Chang, H., D.-Y. Yeung and Y. Xiong. 2004. Super-resolution through neighbor embedding. Pages 275–282 in *Proceedings of the IEEE Computer Society Conference on Computer Vision and Pattern Recognition*.

Chi, M., A. Plaza, J. A. Benediktsson, Z. Sun, J. Shen and Y. Zhu. 2016. Big data for remote sensing: Challenges and opportunities. *Proceedings of the IEEE* 1–13.

Dai, D., Y. Wang, Y. Chen and L. V. Gool. 2016. Is image super-resolution helpful for other vision tasks? *Proceedings of the IEEE Winter Conference on Applications of Computer Vision (WACV).*

Dong, C., C. C. Loy, K. He and X. Tang. 2016. Image super-resolution using deep convolutional networks. *IEEE Transactions on Pattern Analysis and Machine Intelligence* 38:295–307.

He, K., X. Zhang, S. Ren and J. Sun. 2016. Deep residual learning for image recognition. Pages 770–778 in *Proceedings of the IEEE Conference on Computer Vision and Pattern Recognition*.

Huang, N., Y. Yang, J. Liu, X. Gu and H. Cai. 2017. Single-image super-resolution for remote sensing data using deep residual-learning neural network. In *Proceedings of the International Conference on Neural Information Processing*. Cham, Switzerland: Springer.

Jeon, D. S., S.-H. Baek, I. Choi and M. H. Kim. 2018. Enhancing the spatial resolution of stereo images using a parallax prior. Pages 1721–1730 in *Proceedings of the IEEE Conference on Computer Vision and Pattern Recognition*.

Kim, J., J. K. Lee and K. M. Lee. 2016. Deeply-recursive convolutional network for image super-resolution. Pages 1637–1645 in *Proceedings of the IEEE Conference on Computer Vision and Pattern Recognition*.

Kim, J., J. K. Lee K. M. Lee. 2016. Accurate image super-resolution using very deep convolutional networks. Pages 1646–1654 in *Proceedings of the IEEE Conference on Computer Vision and Pattern Recognition*.

Lei, S., Z. Shi and Z. Zou. 2017. Super-resolution for remote sensing images via local–global combined network. *IEEE Geoscience and Remote Sensing Letters* 14:1243–1247.

Li, Y., Y. Zhang, X. Huang, Z. Hu and J. Ma. 2018. Large-scale remote sensing image retrieval by deep hashing neural networks. *IEEE Transactions on Geoscience and Remote Sensing* 56:950–965.

Ling, X., Y. Zhang, J. Xiong, X. Huang and Z. Chen. 2016. An image matching algorithm integrating global SRTM and image segmentation for multi-source satellite imagery. *Remote Sensing* 8 (8):672.

Lu, X., Y. Yuan and P. Yan. 2013. Image super-resolution via double sparsity regularized manifold learning. *IEEE Transactions on Circuits and Systems for Video Technology* 23 (12):2022–2033.

Luo, Y., L. Zhou, S. Wang and Z. Wang. 2017. Video satellite imagery super resolution via convolutional neural networks. *IEEE Geoscience and Remote Sensing Letters* 14:2398–2402.

Ma, Y., H. Wu, L. Wang, B. Huang, R. Ranjan, A. Zomaya and W. Jie. 2015. Remote sensing big data computing: Challenges and opportunities. *Future Generation Computer Systems* 51:47–60.

Mao, X. J., C. Shen and Y. B. Yang. 2016. Image restoration using convolutional auto-encoders with symmetric skip connections. *arXiv* preprint: *arXiv* 1603.09056.

Rottensteiner, F., J. Trinder, S. Clode and K. Kubik. 2005. Using the Dempster–Shafer method for the fusion of LIDAR data and multi-spectral images for building detection. *Information Fusion* 6:283–300.

Sadeghi, Y., B. St-Onge, B. Leblon and M. Simard. 2016. Canopy height model (CHM) derived from a TanDEM-X InSAR DSM and an airborne Lidar DTM in Boreal forest. *IEEE Journal of Selected Topics in Applied Earth Observations and Remote Sensing* 9:381–397.

Schulter, S., C. Leistner and H. Bischof. 2015. Fast and accurate image upscaling with super-resolution forests. Pages 3791–3799 in *Proceedings of the IEEE Conference on Computer Vision and Pattern Recognition*.

Shen, H., X. Meng and L. Zhang. 2016. An integrated framework for the spatio–temporal–spectral fusion of remote sensing images. *IEEE Transactions on Geoscience and Remote Sensing* 54:7135–7148.

Song, H., Q. Liu, G. Wang, R. Hang and B. Huang. 2018. Spatiotemporal satellite image fusion using deep convolutional neural networks. *IEEE Journal of Selected Topics in Applied Earth Observations and Remote Sensing* 11:821–829.

Song, X., Y. Dai and X. Qin. 2016. Deep depth super-resolution: Learning depth super-resolution using deep convolutional neural network. Pages 360–375 in *Proceedings of the IEEE Conference on Computer Vision and Pattern Recognition*.

Sun, J., Z. Xu and H.-Y. Shum. 2008. Image super-resolution using gradient profile prior. Pages 1–8 in *Proceedings of the IEEE Conference on Computer Vision and Pattern Recognition*.

Tai, Y.-W., S. Liu, M. S. Brawn and S. Lin. 2010. Super-resolution using edge prior and single image detail synthesis. Pages 2400–2407 in *Proceedings of the IEEE Computer Society Conference on Computer Vision and Pattern Recognition*.

Taud, H., J. F. Parrot and R. Alvarez. 1999. Dem generation by contour line dilation. *Computers & Geosciences* 25 (7):775–783.

Vedaldi, A. and K. Lenc. 2015. MatConvNet: Convolutional neural networks for MATLAB. Pages 689–692 in *Proceedings of the 23rd ACM International Conference on Multimedia—MM '15*.

Wan, Y. and Y. Zhang. 2017. The P2L method of mismatch detection for push broom high-resolution satellite images. *ISPRS Journal of Photogrammetry and Remote Sensing* 130:317–328.

Wang, Z., J. Chen and S. C. H. Hoi. 2019. Deep learning for image super-resolution: A survey. *Proceedings of the IEEE Conference on Computer Vision and Pattern Recognition*.

Wen, Y., K. Zhang, Z. Li and Y. Qiao. 2016. A discriminative feature learning approach for deep face recognition. Pages 499–515 in *Proceedings of the European Conference on Computer Vision*.

Xia, G.-S., X. Bai, X., J. Ding, J., Z. Zhu, Z., S. Belongie, S., J. Luo, J., M. Datcu, M. Pelillo, M., &and L. Zhang., L. 2018. DOTA: A large-scale dataset for object detection in aerial images. Pages 3974–3983 in *Proceedings of the IEEE Conference on Computer Vision and Pattern Recognition*, 2018, pp.3974 - 3983.

Xu, Z., X. Wang, Z. Chen, D. Xiong, M. Ding and W. Hou. 2015. Nonlocal similarity based dem super resolution. *ISPRS Journal of Photogrammetry and Remote Sensing* 110(Complete):48–54.

Xu, Z., Z. Chen, W. Yi, Q. Gui, W. Hou, and M. Ding. 2019. Deep gradient prior network for DEM super-resolution: Transfer learning from image to DEM. *ISPRS Journal of Photogrammetry and Remote Sensing* 150:80–90.

Yan, W. Y., A. Shaker and N. El-Ashmawy. 2015. Urban land cover classification using airborne LiDAR data: A review. *Remote Sensing of Environment* 158:295–310.

Yang, J., J. Wright, T. Huang and Y. Ma. 2008. Image super-resolution as sparse representation of raw image patches. Pages 1–8 in *Proceedings of the IEEE Conference on Computer Vision and Pattern Recognition*.

Yang, J., J. Wright, T. S. Huang and Y. Ma. 2010. Image super-resolution via sparse representation. *IEEE Transactions on Image Processing* 19:2861–2873.

Zeng, K., J. Yu, R. Wang, C. Li and D. Tao. 2017. Coupled deep autoencoder for single image super-resolution. *IEEE Transactions on Cybernetics* 47:27–37.

Zewei, H., T. Siliang, Y. Jiangxin, C. Yanlong, Y. M. Ying and C. Yanpeng. 2018. Cascaded deep networks with multiple receptive fields for infrared image super-resolution. *IEEE Transactions on Circuits and Systems for Video Technology* 1 (1).

Zhang, H., J. Yang, Y. Zhang and T. S. Huang. 2010. Non-local kernel regression for image and video restoration. Pages 566–579 in *Proceedings of the European Conference on Computer Vision*.

Zhang, K., W. Zuo and L. Zhang. 2018. Learning a single convolutional super resolution network for multiple degradations. Pages 3262–3271 in *Proceedings of the IEEE Conference on Computer Vision and Pattern Recognition*.

Zhang, Y., Y. Wan, X. Huang and X. Ling. 2016. DEM-assisted RFM block adjustment of pushbroom Nadir viewing HRS imagery. *IEEE Transactions on Geoscience and Remote Sensing* 54:1025–1034.

Zhang, Y., Y. Zhang, D. Mo, Y. Zhang and X. Li. 2017. Direct digital surface model generation by semi-global vertical line locus matching. *Remote Sensing* 9 (3): 214.

Zhou, Q. and A. X. Zhu. 2013. The recent advancement in digital terrain analysis and modeling. *International Journal of Geographical Information Science* 27 (7):1269–1271.

Assignment of Copyright to ASPRS

Current copyright law requires that authors of papers submitted for publication in *Photogrammetric Engineering & Remote Sensing* transfer copyright ownership to the American Society for Photogrammetry and Remote Sensing before the paper may be published. Upon receipt of this form with your Master Proof, please complete this form and forward it to the Production Coordinator (address below).

Manuscript Title: A CNN-Based Subpixel Level DSM Generation Approach via Single Image Super-Resolution

Author(s): Yongjun Zhang, Zhi Zheng, Yimin Luo, Yanfeng Zhang, Yi Wan, Jun Wu, Zhiyong Peng and Xiu Liu

Assignment of Copyright in the above-titled work is made on (date) 20/08/2019 from the above listed author(s) to the American Society for Photogrammetry and Remote Sensing, publisher of *Photogrammetric Engineering & Remote Sensing*.

In consideration of the Publisher's acceptance of the above work for publication, the author or co-author(s) hereby transfer(s) to the American Society for Photogrammetry and Remote Sensing the full and exclusive copyright to the work for all purposes for the duration of the copyright. I (we) understand that such transfer of copyright does not preclude specific personal use, provided that prior to said use, permission is requested from and granted by the American Society for Photogrammetry and Remote Sensing.

I (we) acknowledge that this paper has not been previously published, nor is it currently being considered for publication by any other organization.

Author/co-author signatures

Co-authors may fill out and submit this form separately (photocopies are acceptable) if desired; but all co-authors must sign either this or a separate form.

Special Note to U.S. Government Employees

Material prepared by U.S. Government employees as part of their official duties need not have the assignment of copyright transferred since such material is automatically considered as part of the public domain.

If your paper falls within this category please check the appropriate statement and sign below.

_____ This paper has been prepared wholly as part of my (our) official duties as (a) U.S. Government Employee(s). I (we) acknowledge that this paper has not previously been published, nor is it currently being considered for publication, by any other organization.

_____ This paper has been prepared partly in the course of my (our) official duties as (a) U.S. Government Employee(s). For any part(s) not prepared in the course of my (our) official duties, copyright is hereby transferred to the American Society for Photogrammetry and Remote Sensing. I (we) acknowledge that this paper has not previously been published, nor is it currently being considered for publication, by any other organization.

Author/co-author signatures

Please return this form to:
Production Coordinator, ASPRS
5410 Grosvenor Lane, Suite 210
Bethesda, MD 20814-2160
301-493-0290, 301-493-0208 (fax), www.asprs.org

PE&RS Colorplate, Offprint, and Extra Pages Payment Form

This is the only opportunity available to order additional offset printing quality copies of your article. *PE&RS* does not go back on press after the issue's publication. Offprints are only shipped when ordered; they are not complimentary.

However, all authors will receive one complimentary copy of the *PE&RS* issue containing their article and a complimentary PDF of their article. This form should be completed as soon as the initial proof is received, and should be returned with payment for offprints and page charges to ASPRS.

Article Description: Manuscript # 18-125

Article Title: A CNN-Based Subpixel Level DSM Generation Approach via Single Image Super-Resolution

Author(s): Yongjun Zhang, Zhi Zheng, Yimin Luo, Yanfeng Zhang, Yi Wan, Jun Wu, Zhiyong Peng and Xiu Liu

Offprint and Extra Pages Prices

Please refer to the price chart and conditions on the back of this form in order to complete the table below.

Quantity	Description	Amount
	Offprints	0
	Journal Covers (actual issue cover)	0
	Extra Pages @125 per page (each page over 7 journal pages, reference "Instructions to Authors".)	500
	Shipping (applies to offprints and covers only (see price chart and conditions on back of this form.)	0
	Subtotal	

Color Plate Prices*

1-3	4-6	7+
$500	$1,000	$1,500
	Subtotal	1000

* For purposes of this form, a color plate is considered to be a plate that is numbered, even if it contains several parts, e.g. (a), (b), and so on.

Total $ 1500

Author Contact Information:

Name: Yongjun Zhang Email: zhangyj@whu.edu.cn

Affiliation: School of Remote Sensing and Information Engineering, Wuhan University

Street Address: No.129 LuoYu Road

City: Wuhan State/Province: Hubei

Zip Code/Postal Code: 430079 Country: China

Phone: +86-27-68771101 Fax:

Shipping Information (if different from above)**:**

Name:

Affiliation:

Street Address:

City: State/Province:

Zip Code/Postal Code: Country:

Method of Payment:

Accepted manuscripts with color images will not be released for publication until this form is received along with payment. Payments must be made in US dollars, drawn on a US bank, or appropriate credit card. Make checks payable to ASPRS. Keep a copy for your records.

○ Visa ○ MasterCard ○ Discover ○ American Express ◉ Check (print PE&RS issue date & manuscript # on check)

Name on Credit Card: Signature:

Account Number: CSC: Expires (MO/YR):

Phone number for person above: Email Address (for receipt)

SEND this form along with method of payment to:

ASPRS, 425 Barlow Place, Suite 210, Bethesda, MD 20814-2160 rkelley@asprs.org*

*If unable to email credit card information please submit the form without the credit card number and someone from ASPRS will contact you for the information.

Conditions:

Offprints are only shipped when ordered; they are not complimentary. However, all authors will receive one ccomplimentary copy of the PE&RS issue containing their article and a complimentary PDF of their article. Offprint prices are based on the number of pages in an article. Orders are restricted to the quantities listed below. If offprints are not ordered prior to the issue's publication, reprints may be provided in multiples of 100 at the customer's expense. Shipping prices are based on weight and must be added to offprint and journal cover prices for an order to be processed. If overnight delivery is required, customers must provide an account code for the expense of the service (please indicate carrier and account number in the itemized table next to "Shipping").

Prices:

Please enter the price that corresponds to the quantity of offprints and/or covers being ordered on the front of this form.

Offprints and Covers	**25**	50	75	100*
Offprints (1 to 4 page article)	9.00	15.00	21.00	27.00
Offprints (5 to 8 page article)	15.00	27.00	39.00	51.00
Offprints (9 to 12 page article)	21.00	39.00	57.00	75.00
Offprints (13 to 16 page article)	27.00	51.00	75.00	99.00
Journal Covers	9.00	15.00	21.00	27.00
Cover Sponsor (Applies to Outside Front Cover image suppliers only)	475.00 for 1000 covers and TOC			

Shipping Prices:

Domestic (UPS Ground)	25	50	75	100*
Offprints (1 to 4 page article)	7.59	7.98	9.08	8.69
Offprints (5 to 8 page article)	7.98	9.08	9.57	10.53
Offprints (9 to 12 page article)	8.25	9.57	9.79	10.23
Offprints (13 to 16 page article)	8.69	9.79	10.23	11.44
Journal Covers	7.59	7.98	8.25	8.64
Cover Sponsor (Applies to Outside Front Cover image suppliers only)				70.00

Canada (Air Parcel Post)	25	50	75	100*
Offprints (1 to 4 page article)	19.14	20.78	21.45	22.11
Offprints (5 to 8 page article)	20.68	22.11	23.87	25.74
Offprints (9 to 12 page article)	21.45	23.87	26.57	28.82
Offprints (13 to 16 page article)	22.11	25.74	28.85	31.96
Journal Covers	19.14	20.68	21.45	22.11
Cover Sponsor (Applies to Outside Front Cover image suppliers only)	Contact ASPRS for Shipping Prices.			

Mexico (Air Parcel Post)	25	50	75	100*
Offprints (1 to 4 page article)	22.39	23.87	24.75	27.12
Offprints (5 to 8 page article)	24.11	27.12	30.64	34.50
Offprints (9 to 12 page article)	25.52	30.69	36.03	40.26
Offprints (13 to 16 page article)	27.12	34.60	40.26	45.98
Journal Covers	22.33	23.87	25.52	27.12
Cover Sponsor (Applies to Outside Front Cover image suppliers only)	Contact ASPRS for Shipping Prices.			

Overseas (Air Parcel Post)	25	50	75	100*
Offprints (1 to 4 page article)	28.05	30.31	41.69	36.06
Offprints (5 to 8 page article)	30.36	36.03	45.26	47.41
Offprints (9 to 12 page article)	33.17	41.69	49.55	55.99
Offprints (13 to 16 page article)	36.03	47.41	55.99	64.51
Journal Covers	28.05	30.31	41.69	46.03
Cover Sponsor (Applies to Outside Front Cover image suppliers only)	Contact ASPRS for Shipping Prices.			